



(523599) 2003 RM: The Asteroid that Wanted to be a Comet

Davide Farnocchia¹, Darryl Z. Seligman², Mikael Granvik^{3,4}, Olivier Hainaut⁵, Karen J. Meech⁶, Marco Micheli⁷, Robert Weryk⁸, Steven R. Chesley¹, Eric J. Christensen⁹, Detlef Koschny^{10,11,12}, Jan T. Kleyna⁶, Daniela Lazzaro¹³, Michael Mommert¹⁴, and Richard J. Wainscoat⁶

¹ Jet Propulsion Laboratory, California Institute of Technology, 4800 Oak Grove Drive, Pasadena, CA 91109, USA; Davide.Farnocchia@jpl.nasa.gov

² Department of Astronomy and Carl Sagan Institute, Cornell University, 122 Sciences Drive, Ithaca, NY, 14853, USA

³ Asteroid Engineering Laboratory, Luleå University of Technology, Box 848, SE-98128 Kiruna, Sweden

⁴ Department of Physics, PO Box 64, FI-00014 University of Helsinki, Finland

⁵ ESO, Karl-Schwarzschild-Straße 2, D-85748 Garching-bei-München, Germany

⁶ Institute for Astronomy, University of Hawaii, 2680 Woodlawn Drive, Honolulu, HI 96822, USA

⁷ ESA NEO Coordination Centre, Largo Galileo Galilei, 1, I-00044 Frascati (RM), Italy

⁸ Physics and Astronomy, The University of Western Ontario, 1151 Richmond Street, London, ON N6A 3K7, Canada

⁹ Lunar and Planetary Laboratory, University of Arizona, 1629 E University Boulevard, Tucson, AZ 85721, USA

¹⁰ ESA NEO Coordination Centre, Via Galileo Galilei, 1, I-00044 Frascati (RM), Italy

¹¹ ESA ESTEC, Keplerlaan 1, 2201 AZ Noordwijk, The Netherlands

¹² LRT, TU Munich, Boltzmannstraße 15, D-85748 Garching bei München, Germany

¹³ Observatório Nacional, R. Gen. José Cristino, 77, 20921-400 Rio de Janeiro, RJ, Brazil

¹⁴ School of Computer Science, University of St. Gallen, Rosenbergstrasse 30, CH-9000 St. Gallen, Switzerland

Received 2022 December 6; revised 2023 January 9; accepted 2023 January 10; published 2023 February 9

Abstract

We report a statistically significant detection of nongravitational acceleration on the subkilometer near-Earth asteroid (523599) 2003 RM. Due to its orbit, 2003 RM experiences favorable observing apparitions every 5 yr. Thus, since its discovery, 2003 RM has been extensively tracked with ground-based optical facilities in 2003, 2008, 2013, and 2018. We find that the observed plane-of-sky positions cannot be explained with a purely gravity-driven trajectory. Including a transverse nongravitational acceleration allows us to match all observational data, but its magnitude is inconsistent with perturbations typical of asteroids such as the Yarkovsky effect or solar radiation pressure. After ruling out that the orbital deviations are due to a close approach or collision with another asteroid, we hypothesize that this anomalous acceleration is caused by unseen cometary outgassing. A detailed search for evidence of cometary activity with archival and deep observations from the Panoramic Survey Telescope and Rapid Response System and the Very Large Telescope does not reveal any detectable dust production. However, the best-fitting H₂O sublimation model allows for brightening due to activity consistent with the scatter of the data. We estimate the production rate required for H₂O outgassing to power the acceleration and find that, assuming a diameter of 300 m, 2003 RM would require $Q(\text{H}_2\text{O}) \sim 10^{23}$ molec s⁻¹ at perihelion. We investigate the recent dynamical history of 2003 RM and find that the object most likely originated in the mid-to-outer main belt (~86% probability) as opposed to from the Jupiter-family comet region (~11% probability). Further observations, especially in the infrared, could shed light on the nature of this anomalous acceleration.

Unified Astronomy Thesaurus concepts: Asteroid dynamics (2210); Comet dynamics (2213); Near-Earth objects (1092)

1. Introduction

Modeling the trajectory of small bodies is a nontrivial problem. As the data quality improves and observational arcs get extended, nongravitational perturbations can become a significant consideration. Comets are especially affected by nongravitational forces because of the sublimation and outgassing of volatiles (Meech & Svoren 2004). Therefore, orbit determination centers that estimate cometary orbits such as the Jet Propulsion Laboratory¹⁵ and the Minor Planet Center¹⁶ account for nongravitational perturbations in the orbit model. Typically, these perturbations are incorporated based on the standard model of Marsden et al. (1973), although more

sophisticated models (e.g., Yeomans & Chodas 1989; Królikowska 2004; Yeomans et al. 2004; Chesley & Yeomans 2005) are sometimes employed.

As opposed to cometary orbits, the trajectories of asteroids are generally better approximated with a motion purely driven by gravitational forces. In fact, while asteroids are also subject to nongravitational perturbations such as solar radiation pressure (Vokrouhlický & Milani 2000) and the Yarkovsky effect (Vokrouhlický et al. 2015), these are orders of magnitude weaker than forces induced via outgassing. These weaker forces can still be detectable with astrometric data, especially with radar measurements (Ostro et al. 2002) and/or long observational arcs. Solar radiation pressure has been measured for a handful of small near-Earth asteroids (MPEC 2008-D12,¹⁷ Micheli et al. 2012, 2013; Mommert et al. 2014a, 2014b; Micheli et al. 2014; Farnocchia et al. 2017; Fedorets et al. 2020), while searches for detections of the Yarkovsky effect are performed regularly (e.g., Farnocchia et al. 2013;

¹⁵ <https://ssd.jpl.nasa.gov>

¹⁶ <https://minorplanetcenter.net>

¹⁷ <https://www.minorplanetcenter.org/mpec/K08/K08D12.html>

Del Vigna et al. 2018; Greenberg et al. 2020) and have led to hundreds of detections.

Asteroid (523599) 2003 RM was discovered by the Near-Earth Asteroid Tracking Program (Pravdo et al. 1999) on 2003 September 2 (MPEC 2003-R17).¹⁸ 2003 RM has a semimajor axis $a = 2.92$ au and eccentricity $e = 0.60$, which yields apsidal distances of $q \times Q = 1.17$ au \times 4.68 au. The inclination is $10^\circ.9$ relative to the ecliptic plane. Since the initial discovery, there have been over 300 optical observations of 2003 RM over the course of four apparitions in 2003, 2008, 2013, and 2018. While searching for the Yarkovsky effect among near-Earth asteroids, Chesley et al. (2016) detected a clear signal of a transverse acceleration in the motion of 2003 RM. They noted that the observed acceleration was far too large to be caused by the Yarkovsky effect, and argued that cometary activity was the most likely explanation. However, Chesley et al. (2016) also reported that closer inspection of observational images of 2003 RM by a number of near-Earth object search programs (Christensen et al. 2016; McMillan et al. 2016; Wainscoat et al. 2016) did not reveal any clear evidence of cometary activity. To date, no detection of cometary activity has been reported to the Minor Planet Center and therefore 2003 RM currently remains classified as an asteroid.

A similar puzzle affects the understanding of the cometary nature of 1I/‘Oumuamua, the first interstellar object to be discovered passing through the inner solar system (MPECs 2017-U181 and 2017-V17).^{19,20} While no cometary activity was detected around ‘Oumuamua (Meech et al. 2017; Trilling et al. 2018), its astrometric positions could only be explained with the addition of nongravitational perturbations, most plausibly due to outgassing activity (Micheli et al. 2018). Additionally, ‘Oumuamua had an extreme shape, a reddened reflection spectrum (Meech et al. 2017), and a low incoming velocity indicating a young <40 Myr age (Feng & Jones 2018). Reconciling the lack of activity and the observed nongravitational perturbations remains a challenge (Jewitt & Seligman 2022), even though models have been proposed that could explain all the observed properties of ‘Oumuamua, e.g., by assuming a significant presence of molecular hydrogen ice (Seligman & Laughlin 2020). Alternative explanations have invoked the presence of N_2 - and CO-driven activity (Desch & Jackson 2021; Jackson & Desch 2021; Seligman et al. 2021) or radiation pressure (Micheli et al. 2018). Spin-up was detected in the object (Taylor et al. 2022) consistent with outgassing torques (Rafikov 2018). There is precedent for outgassing without dust activity, such as the CO enriched active Centaur 29P/Schwassmann-Wachmann 1 (Senay & Jewitt 1994; Crovisier et al. 1995; Gunnarsson et al. 2008; Paganini et al. 2013), which exhibited CO and dust outbursts that were not well correlated in time (Wierzbos & Womack 2020).

2. Astrometry

2003 RM is currently in a 5:1 mean-motion resonance with the Earth. Subsequently, the object has apparitions visible from the Earth every five years. Since its discovery in 2003, the object has been extensively tracked with ground-based optical facilities over the course of the following four apparitions:

1. From 2003 September 2 to 2003 October 19: 85 observations;
2. From 2008 June 24 to 2008 October 29: 73 observations;
3. From 2013 May 16 to 2013 October 24: 45 observations;
4. From 2018 March 18 to 2018 November 14: 98 observations.

The full observational data set is available from the Minor Planet Center.²¹ For the majority of the existing astrometric data, observations were weighted using the scheme presented by Vereš et al. (2017). Positional uncertainties were estimated for our own measurements:

1. Siding Spring Survey (station code E12)²² observations on 2008 June 24 and 25, which we remeasured and weighted at $0''.5$;
2. Catalina Sky Survey (station code 703) observations on 2008 September 7 (weights at $0''.2$) and 21 ($0''.6$), 2013 August 28 ($0''.8$), 2013 September 15 ($0''.5$) and 23 ($0''.8$), which we remeasured;
3. Panoramic Survey Telescope and Rapid Response System (Pan-STARRS) 1 (station code F51) observations on 2013 July 7 ($0''.2$), 2013 August 17 ($0''.1$) and 28 ($0''.2$), 2013 September 14 ($0''.1$), and 2013 October 24 ($0''.1$);
4. Observatório Astronômico do Sertão de Itaparica, Nova Itacuruba (station code Y28) observations on 2018 March 18 ($0''.7$), 2018 April 19 ($0''.1$) and 20 ($0''.2$), 2018 May 17 ($0''.2$), 2018 July 09 ($0''.2$), 15 ($0''.1$), 17 ($0''.1$), and 18 ($0''.1$), 2018 August 7 ($0''.1$), 2018 September 6 ($0''.1$) and 11 ($0''.2$);
5. Las Campanas Observatory (station code 304), with the Magellan Baade telescope, on 2018 June 22 ($0''.1$);
6. Lowell Discovery Telescope (station code G37) on 2018 September 4 ($0''.15$);
7. Very Large Telescope (VLT; station code 309) with the Unit Telescope 1, observations on 2018 September 19 ($0''.1$).

We assumed a 1 s uncertainty in the reported time of observation and corrected for star catalog systematic errors using the Eggl et al. (2020) debiasing scheme. To reject outliers, we employed the Carpino et al. (2003) algorithm.

3. Detection of Nongravitational Perturbations

Our default gravitational force model configuration (e.g., Farnocchia et al. 2015) is based on JPL planetary ephemeris DE441 (Park et al. 2021) and the 16 most massive small-body perturbers in the main belt (Farnocchia 2021).²³ As was initially pointed out by Chesley et al. (2016), this gravity-only model configuration fails to satisfactorily match the 2003 RM astrometric data. While any given set of two consecutive apparitions can be fit, the addition of a third apparition results in unacceptably high residuals.

To illustrate this point, Figure 1 shows the astrometric residuals of the entire data set against gravity-only solutions based on two consecutive apparitions. Except for a handful of outliers, the residuals of the fitted astrometric observations are consistent with the assumed observational uncertainties.

¹⁸ <https://www.minorplanetcenter.net/mpec/K03/K03R17.html>

¹⁹ <https://minorplanetcenter.net/mpec/K17/K17U11.html>

²⁰ <https://minorplanetcenter.net/mpec/K17/K17V17.html>

²¹ https://minorplanetcenter.net/db_search/show_object?object_id=523599

²² <https://minorplanetcenter.net/iau/lists/ObsCodesF.html>

²³ ftp://ssd.jpl.nasa.gov/pub/eph/small_bodies/asteroids_de441/SB441_IOM392R-21-005_perturbers.pdf

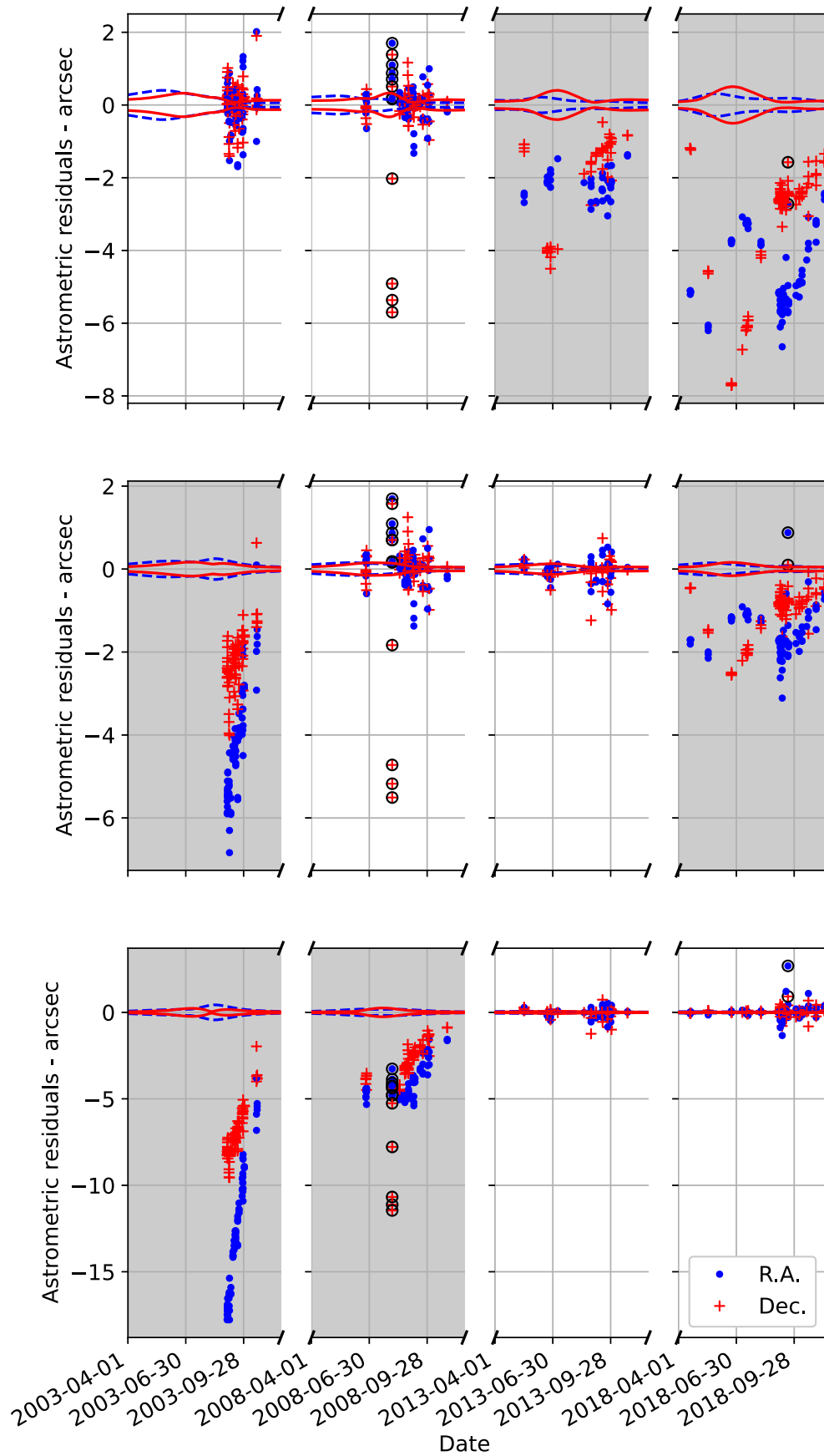


Figure 1. Astrometric residuals against the best gravity-only fit to the astrometry from 2003 to 2008 (top panel), from 2008 to 2013 (middle panel), or from 2013 to 2018 (bottom panel). Dots correspond to R.A. and crosses correspond to decl. Outliers rejected from the fit are indicated with circles. The shaded area corresponds to observations not included in the fit. The dashed line and solid line represent the 1σ ephemeris uncertainties of the orbital solution in R.A. and decl., respectively. The large residuals in the shaded areas far exceed the ephemeris prediction uncertainties and thus imply problems in the force model.

However, residuals of the observations outside the two fitted apparitions are clearly too large to be explained by astrometric errors or ephemeris uncertainties. This behavior is not caused by only a handful of isolated observations. Instead, every apparition has several tens of observations with excessively large residuals. Moreover, the failure to predict astrometric positions manifests for every possible choice of consecutive apparitions included in the fit.

3.1. Yarkovsky Effect

The Yarkovsky effect, a nongravitational perturbation due to the anisotropic thermal reemission of absorbed solar radiation (Vokrouhlický et al. 2015), is a reasonable first explanation for the failure to reproduce the data. In order to model this effect, we include a simple transverse acceleration $A_2(1 \text{ au}/r)^2$, where r is the heliocentric distance and A_2 is an estimable parameter (Farnocchia et al. 2013). The fit to the full observational data set is now satisfactory with a χ^2 of 145.1 and a weighted rms of 0.50. The best fit produces an estimate $A_2 = (212.7 \pm 3.6) \times 10^{-14} \text{ au d}^{-2}$, i.e., a detection with a signal-to-noise ratio of 58. This estimate is consistent when using subsets of the data arc over three apparitions:

1. $A_2 = (212.5 \pm 9.0) \times 10^{-14} \text{ au d}^{-2}$ when fitting the first three apparitions from 2003 to 2013;
2. $A_2 = (207.9 \pm 7.9) \times 10^{-14} \text{ au d}^{-2}$ when fitting the last three apparitions from 2008 to 2018.

Figure 2 demonstrates that fits based on three apparitions that include a transverse acceleration A_2/r^2 successfully predict the fourth apparition within the uncertainties. However, the magnitude of the transverse acceleration far exceeds the magnitude that could feasibly be produced by the Yarkovsky effect. Farnocchia et al. (2013) defined $A_{2,\text{exp}}$ as a proxy for the expected value of $|A_2|$ for a given asteroid. This approximation is derived from the A_2 value measured for (101955) Bennu, scaled according to the expected size of the target asteroid. Bennu is a good reference because of its extreme obliquity and high Yarkovsky detection signal-to-noise ratio. For 2003 RM, the absolute magnitude $H = 19.8$ leads to a range in diameter from 300 to 650 m assuming an albedo between 5% and 25%. Therefore, $A_{2,\text{exp}} < 8 \times 10^{-14} \text{ au d}^{-2}$, which is 27 times smaller than the observed acceleration. Matching the observed acceleration would require either an unrealistically low bulk density ($\sim 0.1 \text{ g cm}^{-3}$) or a size of tens of meters, which requires a nonphysical albedo > 10 .

3.2. Cometary Nongravitational Perturbations

As the Yarkovsky effect is incompatible with the observed acceleration, we considered the possibility that 2003 RM is a comet and that its motion is affected by perturbations due to outgassing. By modeling the transverse acceleration as $A_2g(r)$ (with $g(r)$ from Marsden et al. 1973), we obtain a satisfactory fit to the data. This fit produces $\chi^2 = 138.7$, a weighted rms of 0.49, and $A_2 = (332.4 \pm 5.7) \times 10^{-14} \text{ au d}^{-2}$. In fact, this fit is slightly better than the Yarkovsky solution obtained in the previous subsection. Table 1 shows the corresponding orbit solution. The Tisserand parameter is 2.96, which is in the range between 2 and 3, typical of Jupiter-family comets (Duncan et al. 2004).

We also investigate whether or not the fit to the data favors a specific $g(r) \propto 1/r^m$ power law. Figure 3 shows the best-fit χ^2

as a function of m . There is a very shallow minimum for $m = 9$ with a broad 3σ range ($\Delta\chi^2 = 9$) of acceptable values from $m = 1.6$ to $m = 55$.

There is no signal for the radial component $A_1g(r)$; that is, using the Marsden et al. (1973) model, the estimate of $A_1 = (-2300 \pm 2500) \times 10^{-14} \text{ au d}^{-2}$ is compatible with zero within the uncertainty. The range of possible values for A_1 is compatible with A_1 being an order of magnitude greater than A_2 , which is a typical ratio for comets (Farnocchia et al. 2014a).

3.3. Close Approach to or Collision with Another Asteroid

Another possibility is that the orbit of 2003 RM is perturbed by some other small-body perturber. However, increasing the number of perturbers from 16 to 373 (Farnocchia 2021) neither reveals any significant close approaches nor provides a satisfactory fit to any three of the apparitions. While it is possible that some assumed perturber masses are erroneous, we verified that this could not account for the lack of fit. Specifically, estimating the perturber masses as free parameters within reasonable a priori ranges (similarly to Farnocchia et al. 2021) does not allow a fit to the data. As further proof, the simultaneous estimate of A_2 and the perturber masses still leads to a 58σ detection of A_2 . These results clearly favor the additional nongravitational acceleration over corrections to perturber masses.

With an aphelion of 4.7 au, there is a remote possibility that 2003 RM experienced a close approach or collision with a small body not included as a perturber in the force model. This close approach or collision would more likely have occurred when 2003 RM crossed the main belt, which is densest on the ecliptic plane (e.g., Jedicke et al. 2015; Section 6). However, the ascending and descending nodes of 2003 RM are at 1.2 and 3.6 au from the Sun, respectively. The asteroid distribution has a low density at these distances. Still, the 10° inclination of 2003 RM could allow for close encounters or collisions outside of the ecliptic plane.

The A_2 signal is present when fitting both the first three apparitions and the last three apparitions. Therefore, any close approach and collision would need to take place between the second and the third apparition, i.e., between 2008 October 29 and 2013 May 16. During this time window, we estimated an impulsive velocity variation Δv as a function of time as discussed in Farnocchia et al. (2014b; Section 5). To aid the fit to the data, we included the maximum transverse acceleration allowed by the Yarkovsky effect, i.e., $A_2 = 8 \times 10^{-14} \text{ au d}^{-2}$ (see Section 3.1).

Figure 4 shows the χ^2 of the fit as a function of the epoch during which Δv was applied. There is clear minimum with $\chi^2 = 285.4$ for an impulsive event on 2011 August 19, with a 3σ range from 2011 February 25 to 2012 March 6. We rule out that possibility that an impulsive Δv would explain the deviation from a gravity-only model for the following reasons:

1. During the time frame surrounding the minimum of χ^2 , 2003 RM travels from 4.7 to 4.1 au from the Sun and from 0.5 to 0.1 au above the ecliptic plane. Because this region of the solar system has a low density of asteroids (Lagerkvist & Lagerros 1997; Jedicke et al. 2015), it is extremely unlikely that an impulsive Δv event occurred there.
2. The χ^2 of the fit is significantly higher ($\Delta\chi^2 \sim 147$) than that obtained with the transverse nongravitational acceleration model. This is true despite the fact that a larger

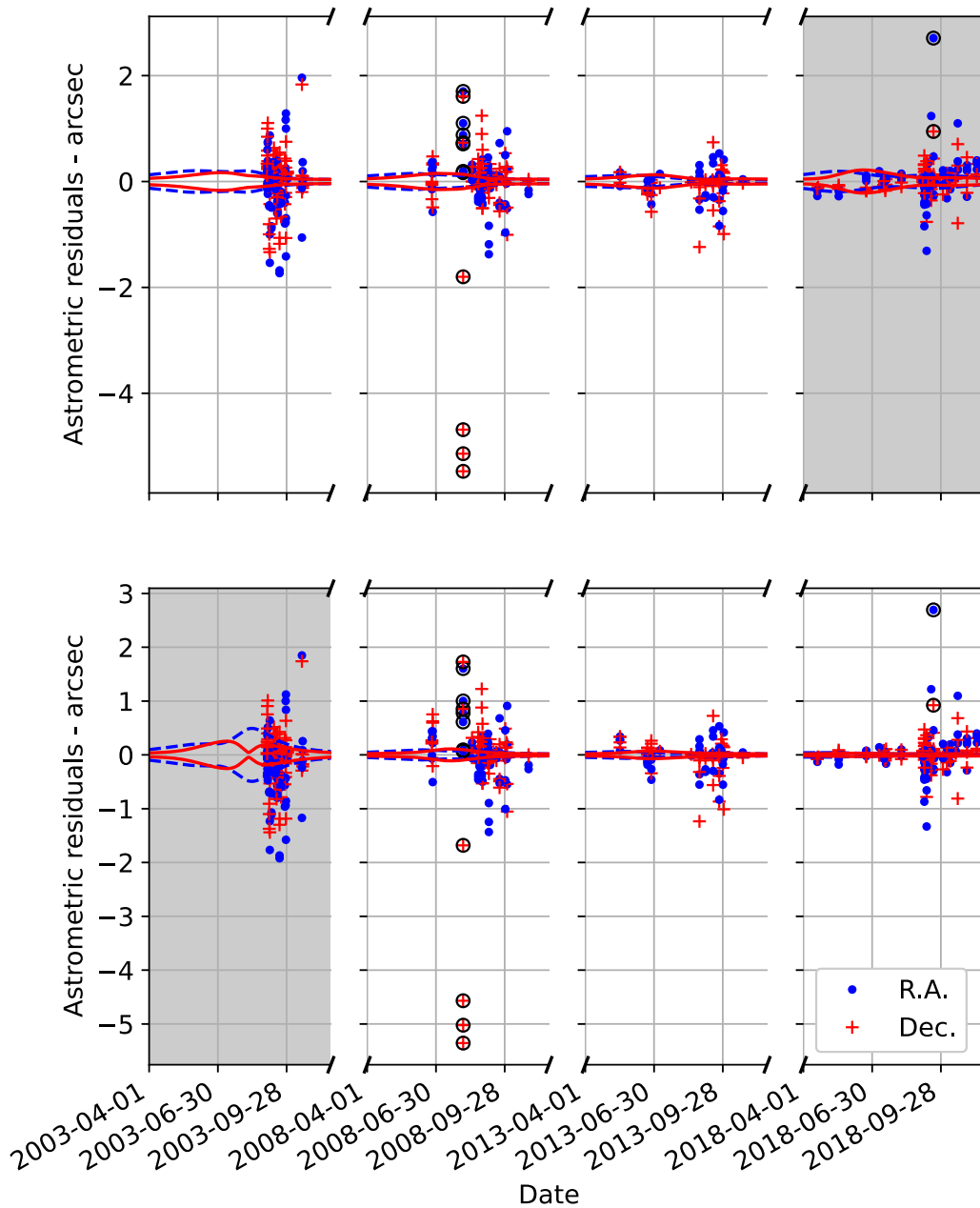


Figure 2. Astrometric residuals against the best fit to the astrometry either from 2003 to 2013 (top panel) or from 2008 to 2018 (bottom panel) using a transverse acceleration A_2/r^2 . Dots correspond to R.A. and crosses correspond to decl. Outliers rejected from the fit are indicated with circles. The shaded area corresponds to observations not included in the fit. The dashed line and solid line represent the 1σ ephemeris uncertainties of the orbital solution in R.A. and decl., respectively. The residuals in the shaded areas are compatible with the ephemeris prediction and thus suggest that the adopted nongravitational model is compatible with the data set.

Table 1

JPL Orbit Solution 58 for 2003 RM using the Marsden et al. (1973) $g(r)$ Function

Parameter	Value	Uncertainty	Units
Eccentricity	0.601 349 357 1	2.39×10^{-8}	
Perihelion distance	1.164 243 531 3	6.98×10^{-8}	au
Time of perihelion TDB	2018 July 4.679 174 4	1.08×10^{-5}	day
Longitude of node	336.725 343 77	9.65×10^{-6}	$^\circ$
Argument of perihelion	324.546 104 0	1.20×10^{-5}	$^\circ$
Inclination	10.861 029 45	3.75×10^{-6}	$^\circ$
A_2	332.42×10^{-14}	5.68×10^{-14}	au d $^{-2}$

Note. The heliocentric orbital elements refer to an osculating epoch of 2017 May 5 TDB and are in the IAU76 ecliptic frame (Seidelmann 1977). The error bars correspond to 1σ formal uncertainties.

number of parameters were used: four (epoch and components of Δv) instead of one (A_2).

3. A three-apparition orbit solution with Δv estimated provides poor predictions for the fourth apparition. For example, Figure 5 shows the astrometric residuals against a solution based on the last three apparitions that estimates a Δv on 2011 August 19. The residuals of the 2003 apparitions are much larger than the ephemeris prediction uncertainties.

4. Search for Evidence of Cometary Activity

No observer has reported a clear detection of cometary activity for 2003 RM to the Minor Planet Center. As a result

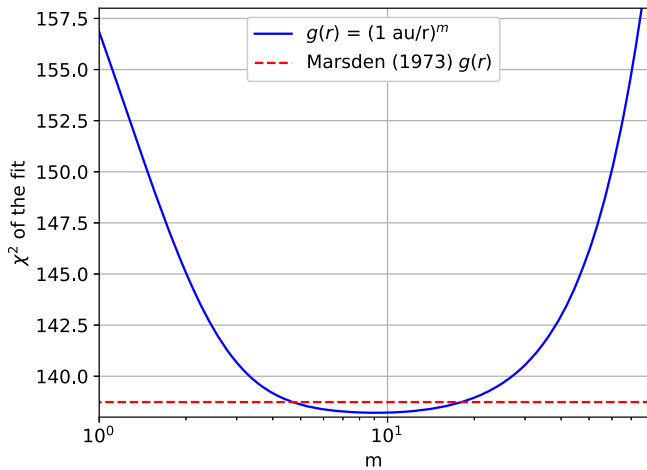


Figure 3. χ^2 of the orbital fit as a function of the power-law exponent for $g(r) = 1/r^m$. The full observational arc is included in the fit, and A_2 is the only nongravitational parameter estimated. The dashed line corresponds to the Marsden et al. (1973) $g(r)$.

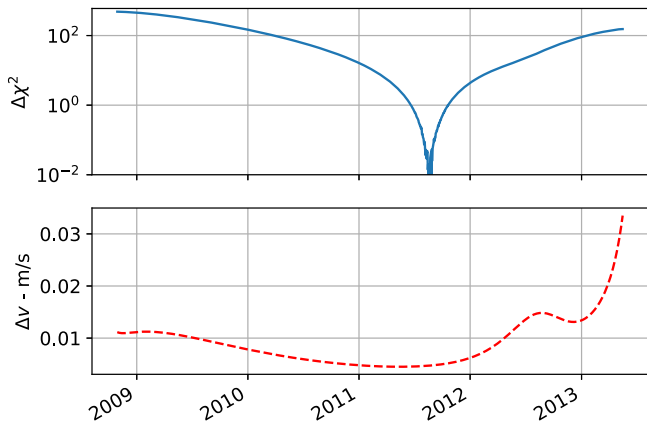


Figure 4. Top panel: $\Delta\chi^2$ of the orbital fit for an orbital solution with an impulsive variation in the velocity Δv as a function of the impulse time relative to the lowest $\chi^2 = 285.4$, which corresponds to a Δv on 2011 August 19. Bottom panel: magnitude of Δv as a function of the impulse time.

2003 RM is classified as an asteroid. We carefully reviewed our observations (see Section 2) and 2003 RM appears stellar in all of them, thus providing no observational evidence of a cometary nature for this object. Below we provide a detailed analysis for two of the observations with the highest signal-to-noise ratio (S/N): Pan-STARRS observations on 2013 August 17, 34 days past perihelion, when 2003 RM was at a heliocentric distance of 1.2 au, and VLT observations on 2018 September 19, 76 days past perihelion, when 2003 RM was at a heliocentric distance of 1.5 au.

4.1. Pan-STARRS

We searched the image archive of the 1.8 m Pan-STARRS1 telescope (Chambers et al. 2016; Wainscoat et al. 2020) located on Maui, Hawai‘i. We inspected the “chip” images of all matching exposures for low-level cometary activity. These images are normally “warped” to a common fixed plane-of-sky projection with $0''.25$ pixels (to allow for deep stacks for nonasteroid science) for survey operations, but using them allows for inspection of the native $0''.256$ pixel data without resampling, which can be useful in identifying subpixel coma.

We employed the Vereš et al. (2012) algorithm to fit the point-spread function (PSF) of both 2003 RM and all visible field stars that appear in the Gaia data release 2 (DR2; Gaia Collaboration et al. 2018) catalog. The FWHM was the primary metric to search for activity. The fit primarily uses an asymmetric Gaussian function and adopts a trailed Gaussian for fast-moving objects. This method also reports uncertainties in the fit. For trailed PSFs, the FWHM corresponds to the direction perpendicular to the motion. The “curve-of-growth” aperture flux (essentially a plot of aperture flux as a function of the aperture radius) is dependent on the PSF of a given object and, for large-enough radii, allows for the identification of faint coma when compared to comparably bright field stars, which do not show such coma.

Unfortunately, there do not exist many Pan-STARRS images for 2003 RM. However, the images with higher SNR show it to be consistent with a star-like appearance. On 2013 August 17, a 60 s z -band image with SNR ~ 15 had an FWHM of $1''.01 \pm 0''.03$ measured perpendicular to the direction of motion. As the plane-of-sky motion of 2003 RM was aligned to the stellar minor axis (i.e., there is a slight asymmetry in the PSFs), the major axis FWHM of $0''.99 \pm 0''.06$ must be used for comparison. The object was too trailed for a curve-of-growth comparison and is illustrated in Figure 6. On 2013 September 14, a 43 s g -band image with SNR ~ 8 had an FWHM of $1''.22 \pm 0''.05$, with the motion of 2003 RM aligned with the stellar major axis. The stellar FWHM minor axis for comparison was $1''.24 \pm 0''.11$. On 2013 October 24, a pair of 45 s i -band images with SNR ~ 6 were stacked to have an FWHM of $1''.01 \pm 0''.05$ (minor axis) and $1''.09 \pm 0''.06$ (major axis) compared to stellar FWHM $1''.00 \pm 0''.06$ and $1''.15 \pm 0''.04$ respectively. The curve of growth in each image was comparable, although the object was fainter than the field stars. On 2018 October 17, a 45 s w -band image with SNR ~ 8 had an FWHM of $1''.38 \pm 1''.06$ (minor axis) and $1''.58 \pm 0''.07$ (major axis) evidently consistent with the stellar FWHM of $1''.33 \pm 0''.06$ and $1''.49 \pm 0''.06$, respectively. The curve-of-growth was consistent with field stars of similar brightness.

Based on these images, there is no evidence of a nonstellar appearance, and an object like this would never be reported even as a marginal comet candidate.

4.2. Very Large Telescope

On 2018 September 19, 2003 RM was observed with the Unit Telescope 1 of the ESO VLT on Paranal, Chile, with the FOcal Reducer and low dispersion Spectrograph 2 (FORIS2; Appenzeller et al. 1998). These observations did not use a filter in order to reach the deepest possible magnitude and surface brightness for an object with solar color. A total of 82 randomly dithered exposures of 40 s were acquired in service mode on 2018 September 19. They were bias- and flat-corrected (with a twilight flat) and normalized to an exposure time of 1 s. Remaining low-spatial-frequency residuals were removed by dividing the frames again by a “super-flat field.” This was obtained using a median of the science frames—after normalization of the sky level around the expected position of the object and masking the background objects.

These frames were then coaligned using a dozen field objects as reference. A master “star” stack was produced, which was used to calibrate the field astrometrically using stars from the Gaia DR2 catalog (Gaia Collaboration et al. 2016, 2018). The expected pixel position of 2003 RM on each frame was computed. The master star stack was then subtracted from each of the individual frames. This subtraction produced images in

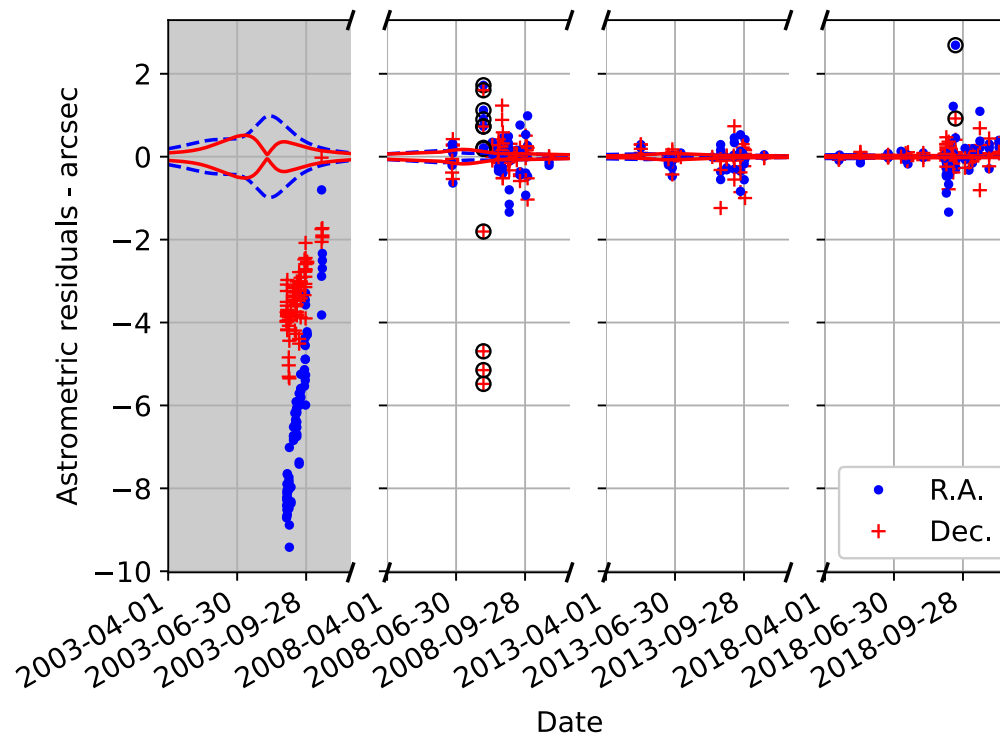


Figure 5. Astrometric residuals against the best fit to the astrometry from 2008 to 2018 with an impulsive Δv event on 2011 August 9. Dots correspond to R.A. and crosses correspond to decl. Outliers rejected from the fit are indicated with circles. The shaded area corresponds to observations not included in the fit. The dashed line and solid line represent the 1σ ephemeris uncertainties of the orbital solution in R.A. and decl., respectively. The large residuals in the shaded areas far exceed the ephemeris prediction uncertainties and thus imply problems in the force model.

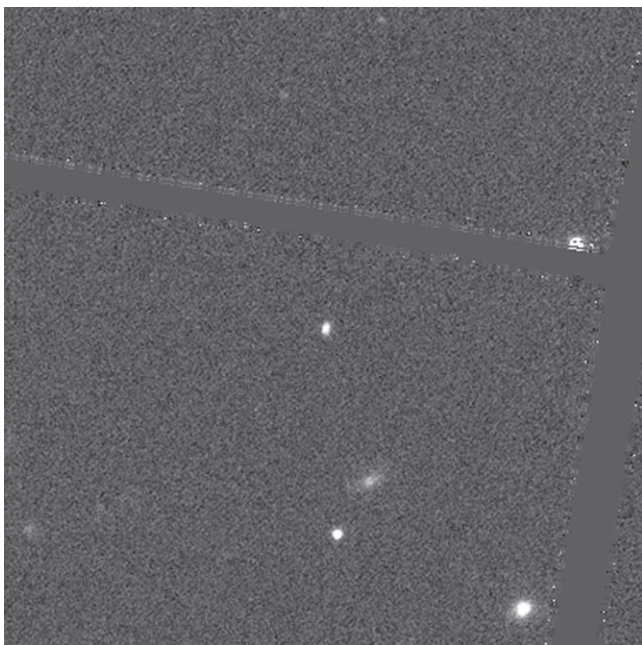


Figure 6. 2003 RM (in the center, north is up, east is left) as it appeared on 2013 August 17 from Pan-STARRS1 moving north at 0.62 degrees per day toward a cell gap. Comparison of the FWHM with visible stars in a larger region than shown here indicates it was not active. At the observation time, 2003 RM was at 1.2 au from the Sun and 0.3 au from Earth.

which the majority of the contribution from background objects was removed. The original and star-subtracted frames were then stacked after being recentered on the expected position of the object, using an average with outlier rejection. Another stack was produced, including only the 55 exposures where the

expected position of the object was at least $10''$ from a background object.

Both the total stack of star-subtracted frames (displayed in Figure 7) and the partial ones (totalling 3280 and 2200 s exposure time, respectively) were searched for dust. Visual inspection of the frame reveals no visible extension of the object.

A photometric profile of 2003 RM was produced by integrating its light in a series of circular apertures centered on the object with increasing radii. The instrumental fluxes in these apertures were converted to surface brightness in the concentric rings. These were then converted to magnitudes using a photometric zero-point of 27.8 (from Hainaut et al. 2021, for filter-less observations). The profile of a field star slightly brighter than 2003 RM was obtained in a similar manner from the “star” stack, and scaled to the brightness of the object for comparison. These profiles are presented in Figure 7, showing no divergence down to $28 \text{ mag arcsec}^{-2}$.

To quantify the lack of dust, it is worth noting that the profile of the object is perfectly stellar within the noise level. Dust contributing to up to 5σ could exist within the error bars. Integrating the corresponding flux from $0''.5$ to $2''$ corresponds to a total magnitude of 24.0. Assuming dust grains with a radius of $1 \mu\text{m}$ and with a density of 3000 kg m^{-3} and an albedo of 0.2, we derive a coma mass limit below 4 kg. This limit should be taken as an order of magnitude estimate based on the numerous assumptions.

5. Heliocentric Light-curve Modeling

Evidence of cometary activity in the form of scattered light from the dust and nucleus can be found from the shape of the heliocentric light curve even in the absence of imaged dust. This can occur when there is brightening caused by light

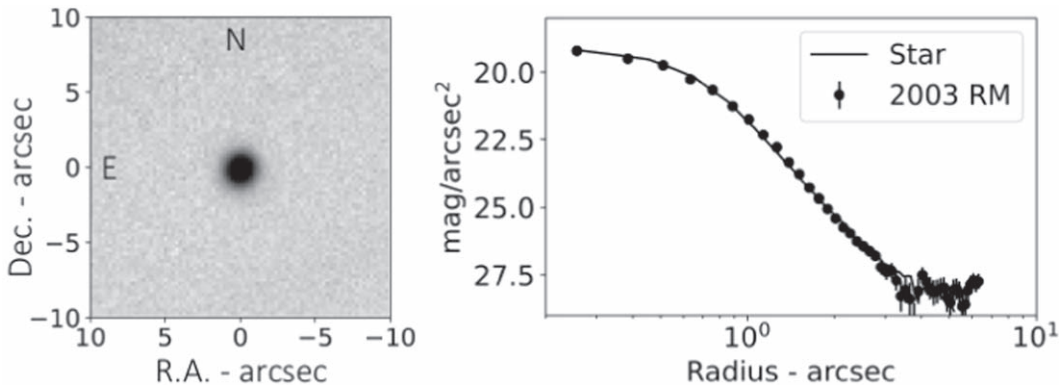


Figure 7. Left: Stack of 82 VLT frames totalling a 3280 s exposure time on 2003 RM. The observations were collected on 2018 September 19, when 2003 RM was at 1.2 au from the Sun and 0.3 au from Earth. The image is $20''$ wide. The individual frames were subtracted for background objects. Right: Surface brightness profile of 2003 RM (dots) and of a scaled field star (line).

scattered from dust contained within the seeing disk, as in the case of a gravitationally bound dust coma such as the inner coma of (2060) Chiron (Meech & Belton 1990) and perhaps (468861) 2013 LU28 (Slomp et al. 2022) and (418993) 2009 MS9 (Bufanda et al. 2022).

To derive limits on outgassing, we used the ice sublimation model to compare the heliocentric light-curve brightness to a predicted comet dust production from outgassing. The model computes the amount of gas sublimating from an icy surface exposed to solar heating, as described in detail in Meech et al. (2017). The total brightness within a fixed aperture combines radiation scattered from the nucleus and dust entrained in the sublimating gas flow and dragged from the nucleus. The model free parameters include the ice type, nucleus radius, albedo, emissivity, density, dust properties (sizes, density, phase function), and fractional active area. 2003 RM has not been well-characterized so we have significant uncertainties for all of these parameters.

We used magnitudes from 329 observations as reported to the Minor Planet Center between 2003 September and 2018 November to model the heliocentric light curve. These data represent observations from 34 different observatories reported using several different photometric systems, including some sets with no filter listed. In order to convert all the measurements to a Sloan Digital Sky Survey (SDSS) r band, we need to know the surface color (e.g., the taxonomic class) for 2003 RM. Most Near-Earth Objects (NEOs) belong to the S taxonomic class (Ieva et al. 2020), and based on this assumption we used the mean SDSS colors from Ye et al. (2016) and the transformations from Jordi et al. (2010) and Lupton (2005)²⁴ to convert the G , V , and R filters to the SDSS r band. Because there was significant scatter in the data (which was likely never intended to represent high-precision photometry), we averaged data points taken on the same night. Data from five of the observing stations were significantly discrepant with observations taken at the same time and were not used. The resulting photometry is shown in Figure 8 and has an error of ~ 0.3 mag (about the size of the data points).

In Section 7 we show that 2003 RM may be associated with the Eos family, which maps to the K-taxonomic class, a subset of the S-type members. These asteroids tend to have the same visible colors as S-type asteroids but slightly lower albedos, around $p_v \sim 0.12$ (Clark et al. 2009). Table 2 lists the

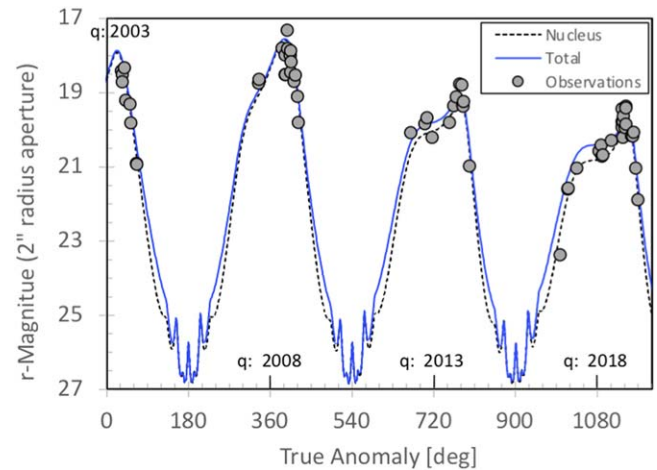


Figure 8. The best-fitting H_2O -sublimation model allows for brightening due to activity consistent with the scatter in the data. The photometric data cover the four observing apparitions from 2003 to 2018 described in Section 2.

starting parameters for the model, along with the references for the starting values. Some of these are based on estimates for S-type asteroids and others are relevant to active comets.

A good fit to the data is shown in Figure 8, and the fit parameters are shown in Table 2 for water. Because of all the nucleus uncertainties, we varied R_N , β_{nuc} , and FAA. The total curve is the brightness combined from the nucleus and the dust lifted off by the water sublimation model. In Figure 8, the nucleus brightness is the best fit to the data, and the “total” model includes scattered light from the nucleus and the dust coma. The model is shown plotted against true anomaly (TA = 0° is at perihelion). Because the data span four apparitions, TA increases by 360° at each perihelion. The VLT data were taken about 2.5 months post-perihelion, at TA = 1144° . The total model curve allowing for activity is consistent with the envelope of the scatter in the data. The implied dust production rate at perihelion for the fourth apparition from this model is 0.114 kg s^{-1} and converting this to a gas production rate assuming a dust-to-gas ratio of 1 (Marschall et al. 2020) gives an inferred $Q(\text{H}_2\text{O}) \sim 3.8 \times 10^{24} \text{ molec s}^{-1}$.²⁵ If the photometric scatter were much

²⁴ <https://classic.sdss.org/dr4/algorithms/sdssUBVRITransform.html#Lupton2005>

²⁵ We have no knowledge of the dust-to-gas ratio. If the dust-to-gas ratio were larger than the model would produce more dust per unit of gas production. The light curve in Figure 8 is a measurement of scattered light from the nucleus and dust. A larger dust-to-gas ratio would imply lower estimates for the gas.

Table 2
Summary of Sublimation Model Parameters

Sublimation Parameter		Initial		Fit		
		Value	Source ^a	H ₂ O	CO ₂ Limit	CO Limit
Nucleus Radius [km]	R_N	0.150	[1]	210	210	210
Emissivity	ϵ	0.95	[2]	0.9	0.9	0.9
Nucleus Phase function [mag deg ⁻¹]	β_{nuc}	0.04	[3]	0.05	0.05	0.05
Nucleus Density [kg m ⁻³]	ρ_n	1900	[4]	1900	1900	1900
Nucleus Albedo	p_v	0.25	[1]	0.12	0.12	0.12
Coma Phase function [mag deg ⁻¹]	β_{coma}	0.02	[5]	0.02	0.02	0.02
Grain Density [kg m ⁻³]	ρ_g	3000	[6]	3000	3000	3000
Grain Radius [μm]	a	1	[7]	1	1	1
Fractional Active Area	FAA	0.04	[7]	0.003	0.000 06	0.000 2
Inferred Gas Production [molec s ⁻¹]	Q			3.8E24	1.7E23	7.3E23

Note.

^a [1] matches the observed H value for high-albedo S-type asteroids; [2] measured for 67P by Rosetta (Spohn et al. 2015); [3] measured for an S-type asteroid (Gehrels & Taylor 1977); [4] average density for small S-type asteroids (25143) Itokawa, (101955) Bennu, (162173) Ryugu, (65803) Didymos); [5] measured for comets (Meech & Jewitt 1987); [6] see discussion in Meech et al. (1997); [7] assumed starting values for comets.

smaller (e.g., less than 0.01 mag), then the model would be sensitive to activity at the level of $\sim 10^{23}$ molec s⁻¹. At this gas production level the integrated brightness from 1 μm dust contained within a 2'' radius aperture would have an r mag of 24, consistent with the limits from the VLT data. This limit is just above the amount of gas production that is required for a nucleus of this size and density based on the nongravitational accelerations (see Figure 9 below).

In order to assess how much of the scatter in the data might be due to the object's rotation, we examined the time-series individual images taken over 2 hr from the VLT on 2018 September 19. We used the flattened sky-subtracted frames and excluded the frames where 2003 RM was too close to field stars (during the first hour). The remaining data show a brightness variation of ~ 0.05 mag with about 14 cycles over a span of 50 minutes that, if statistically significant, would suggest a rapid rotation period of 2003 RM. More data would be necessary to investigate this further.

These models were run on the assumption that a body this small may no longer contain ices as volatile as CO₂ or CO, and the gas production rate limits, which are lower than that for water, are also shown in Table 2. However, as discussed in Section 7, the dynamical lifetime of NEOs on orbits like that of 2003 RM is relatively short. Comet 2P/Encke has an even smaller perihelion than 2003 RM ($q = 0.33$ au) with a slightly larger aphelion ($Q = 4.09$ au). Comet Encke could have migrated in and become decoupled from Jupiter on a similar timescale. Comet Encke exhibits a curious behavior: near perihelion it often has very little visible dust but significant gas, and is often active at aphelion (Meech et al. 2001; Fink 2009). However, this comet still has a very strong CO₂ or CO production (Reach et al. 2013). For both CO₂ and CO, similar limiting production rates of $< 10^{24}$ molec s⁻¹ are found based on the heliocentric light curve.

6. Required Outgassing Production

We consider a variety of assumptions regarding the nature of the outgassing. The production depends on several unconstrained factors, including the albedo (and corresponding size) of the body, the temperature of the outgassing gas, the extent to which the outflowing gas is collimated versus isotropic, and the dust-to-gas mass ratio.

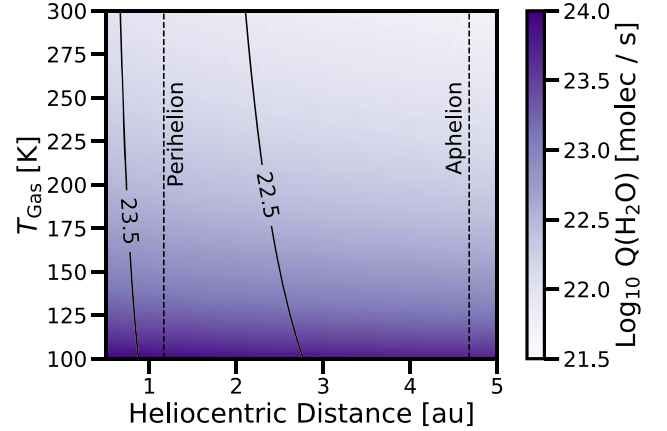


Figure 9. H₂O production rates required to produce the measured nongravitational acceleration of 2003 RM. We calculate this value using Equations (1) and (2), with $\zeta = 1$, radius of 210 meters, $\rho_{\text{Bulk}} = 1.9$ g cm⁻³ and $A_2 = 213.7 \times 10^{-14}$ au d⁻² for a $(r/1 \text{ au})^{-2}$ dependency on the heliocentric distance r .

The production rate $Q(X)$ of a given species, X , can be calculated via the conservation of linear momentum—essentially just the “rocket” equation—using the following equation:

$$Q(X) = \left(\frac{M_{\text{Tot}}}{m_X} \right) \left(\frac{|\ddot{\mathbf{r}}|}{v_{\text{Gas}} \zeta} \right). \quad (1)$$

In Equation (1), the total mass is given by $M_{\text{Tot}} = \rho_{\text{Bulk}} V$, where ρ_{Bulk} and V are the bulk density and the volume of the nucleus. $\ddot{\mathbf{r}}$ is the instantaneous acceleration at the heliocentric position. m_X is the mass of the outgassing molecule and v_{Gas} is the gas outflow velocity. v_{Gas} can be related to the temperature of the outflowing species by equating the kinetic energy to the thermal energy, which is calculated using:

$$v_{\text{Gas}} = \left(\frac{8k_B T_{\text{Gas}}}{\pi m_X} \right)^{1/2}. \quad (2)$$

In Equation (2), T_{Gas} is the temperature of the outgassing species. In Equation (1), the factor ζ parameterizes the geometry of the outgassing species. $\zeta = 1$ corresponds to a

fully collimated outflow, and $\zeta = 0.5$ corresponds to an entirely isotropic hemispherical outflow. For a complete definition of the parametric ζ function, see Section 4.1 in Jewitt & Seligman (2022).

With this construction, we calculate the production rate required to produce the measured nongravitational acceleration under the assumption of a pure H_2O outgassing. We show the resulting production rates for a range of outgassing temperature and heliocentric distance in Figure 9. In order to calculate this production, we assume that the outflow is completely collimated and $\zeta = 1$, a spherical nucleus with radius of $R_{\text{Nuc}} = 210$ m, a bulk density of $\rho_{\text{Bulk}} = 1.9 \text{ g cm}^{-3}$, and a best-fit nongravitational acceleration of $A_2 = 213.7 \times 10^{-14} \text{ au d}^{-2}$ for a $(r/1 \text{ au})^{-2}$ dependency on the heliocentric distance.

This production rate calculation can easily be generalized to other assumptions of the outflow and its composition. The following scaled equation:

$$Q(X) \simeq 2.4 \times 10^{23} \text{ molec s}^{-1} \left(\frac{\rho_{\text{Bulk}}}{1.9 \text{ g cm}^{-3}} \right) \left(\frac{R_{\text{Nuc}}}{210 \text{ m}} \right)^3 \left(\frac{m_{\text{H}_2\text{O}}}{m_X} \right)^{1/2} \left(\frac{1}{\zeta} \right) \left(\frac{100 \text{ K}}{T_{\text{Gas}}} \right)^{1/2} \left(\frac{|A_2|}{213.7 \times 10^{-14} \text{ au d}^{-2}} \right) \left(\frac{1 \text{ au}}{r} \right)^2 \quad (3)$$

may be used to estimate production rates for a variety of assumptions.

7. Dynamical History

2003 RM is currently located adjacent to the Eos family in terms of its semimajor axis and inclination. Therefore, the most likely source region for the object is in the mid-to-outer part of the main asteroid belt or among Jupiter-family comets. We used the medium resolution version of the evolutionary NEO population model by Granvik et al. (2018) to quantify our assessment of the source region. The NEO population model allows us to estimate the relative likelihood that 2003 RM would have entered the NEO region through one of the seven escape regions described by that model. The input for the model assessment are 2003 RM's orbital elements (a , e , i) and absolute magnitude (H). According to this model, 2003 RM has an $(86 \pm 4)\%$ and $(11 \pm 4)\%$ probability of originating in the mid-to-outer asteroid belt and Jupiter-family comet region, respectively. An origin in the inner part of the asteroid belt, including the Hungaria or Phocaea groups, is less likely, with a probability of less than 4% in total. Thus, it appears that an asteroidal origin is more likely than a cometary origin for 2003 RM. It is worth pointing out that a main-belt origin is not necessarily incompatible with a cometary nature. In fact, Hsieh et al. (2020) show how Jupiter-family comets can originate in the main belt.

We used the model developed by Toliou et al. (2021) to assess 2003 RM's orbital history and lower perihelion distance, q . Based on the orbital elements and absolute magnitude, the model predicts that 2003 RM attained $q < 1$ au and $q < 0.5$ au with a probability of $(42 \pm 2)\%$ and $(5 \pm 2)\%$, respectively. Therefore, it is likely that 2003 RM has never experienced heating beyond that it would have been exposed to at about 0.5 au.

How much solar heating and volatile release are likely to have occurred in 2003 RM's past? The average lifetime of

NEOs originating in the mid-to-outer asteroid belt is 300–400 kyr. Approximately 80% of these NEOs will eventually be ejected from the inner solar system as a result of a close encounter with Jupiter (Granvik et al. 2018). The median duration of the time that an object—currently with a 2003 RM-like orbit—spends on orbits with $q < 0.5$ au, $q < 1$ au, and $q < 1.3$ au is about 40, 100, and 190 kyr, respectively (Toliou et al. 2021). Because only a small fraction of the total orbital period occurs close to perihelion, these median times should be reduced by orders of magnitude to estimate the time spent at heliocentric distances $r < 0.5$ au, $r < 1$ au, and $r < 1.3$ au, respectively. If 2003 RM initially contained volatiles, it is possible that the object retained some fraction of them while being an NEA based on these timescales. Moreover, it is believed that main-belt comets that are typically found in the mid-to-outer asteroid belt initially contained volatiles. Therefore, the excess nongravitational acceleration measured for 2003 RM could be caused by weak activity. This is similar to what might have occurred on 11/'Oumuamua.

8. Conclusions

Based on an observation arc from 2003 to 2018, it is clear that the motion of near-Earth asteroid 2003 RM is affected by significant nongravitational perturbations in the transverse direction. Although transverse nongravitational accelerations on asteroids are typically caused by the Yarkovsky effect, the magnitude of the required anomalous acceleration is much greater than can be explained by this phenomenon. We investigated and ruled out alternative explanations for the observed orbital deviations such as close approaches or a collision with another asteroid. Therefore, we conclude that the most likely source of this nongravitational perturbation seems to be some form of cometary outgassing, orders of magnitude smaller than what is typically observed in comets, and that 2003 RM could be a cometary object. (See Extended Data Figure 1 from Micheli et al. 2018 and Figure 4 from Farnocchia et al. 2014a.)

However, direct imaging does not reveal any indication of cometary activity, and even a statistical analysis of the dynamical history of 2003 RM favors an asteroidal origin. If 2003 RM is actively sublimating, it is curious that the object does not display a bright cometary tail. We performed a detailed search through observational data, especially from Pan-STARRs and the VLT, and we found no evidence for extended coma or brightening events in the secular light curve. Therefore, if this object is sublimating, the dust coma is very weak or nonexistent.

We estimated the required levels of H_2O outgassing that would be required to produce the nongravitational perturbations. By invoking the conservation of linear momentum, we estimated that 2003 RM requires production rates of order $Q(\text{H}_2\text{O}) \sim 10^{22}\text{--}10^{23} \text{ molec s}^{-1}$. We also compared the photometric light curve of 2003 RM with a model of (i) a bare nucleus and (ii) a nucleus with the addition of scattered light from a dust coma contained within the unresolved seeing disk. We found that the scatter in the data could be explained by an inferred outgassing rate of $Q(\text{H}_2\text{O}) < 10^{24} \text{ molec s}^{-1}$, a limit just above the amount of gas production required to produce the nongravitational perturbations. Therefore, it is possible but not definitive that 2003 RM could be exhibiting a low level of activity. As a point of reference, the upper limit for main-belt comet water outgassing near perihelion is between 10^{24} and $10^{26} \text{ molec s}^{-1}$ (Snodgrass et al. 2017).

With the information currently available, the nature of 2003 RM remains a puzzle, and it is not clear if the object should be














considered as an asteroid or a comet, if not as a new class of small body in the solar system. 2003 RM is not alone in this regard. In an accompanying paper (Seligman et al. submitted), we report the discovery of similar nongravitational accelerations in six other small objects in the solar system. Even more strikingly, the first discovered interstellar object II/‘Oumuamua also had a significant nongravitational acceleration but no coma.

Additional observations of 2003 RM are necessary to understand the origin of the detected large nongravitational perturbations, which could in turn help solve the similar puzzle on ‘Oumuamua’s nature. Specifically, high signal-to-noise ratio space-based near- and mid-infrared observations could be sensitive to detection H₂O, CO₂ and CO outgassing activity even in the absence of micron-sized dust particles. Observations with the James Webb Space Telescope would be particularly helpful for identifying the source of the acceleration of 2003 RM.

Part of this work was carried out at the Jet Propulsion Laboratory, California Institute of Technology, under a contract with the National Aeronautics and Space Administration (80NM0018D0004). DZS acknowledges financial support from the National Science Foundation Grant No. AST-17152, NASA Grant No. 80NSSC19K0444, and NASA contract NNX17AL71A from the NASA Goddard Space Flight Center. K.J.M. and J.T.K. acknowledge support through an award from the National Aeronautics and Space Administration under grant NASA-80NSSC18K0853. This research has made use of data and/or services provided by the International Astronomical Union’s Minor Planet Center. This research has made use of observations collected at the European Southern Observatory under ESO program 2101.C-5049(A). Pan-STARRS is supported by the National Aeronautics and Space Administration under grant No. 80NSSC18K0971 issued through the SSO Near-Earth Object Observations Program.

Copyright 2023. California Institute of Technology.

ORCID iDs

Davide Farnocchia  <https://orcid.org/0000-0003-0774-884X>
 Darryl Z. Seligman  <https://orcid.org/0000-0002-0726-6480>
 Mikael Granvik  <https://orcid.org/0000-0002-5624-1888>
 Olivier Hainaut  <https://orcid.org/0000-0001-6952-9349>
 Karen J. Meech  <https://orcid.org/0000-0002-2058-5670>
 Marco Micheli  <https://orcid.org/0000-0001-7895-8209>
 Robert Weryk  <https://orcid.org/0000-0002-0439-9341>
 Steven R. Chesley  <https://orcid.org/0000-0003-3240-6497>
 Detlef Koschny  <https://orcid.org/0000-0001-8690-3507>
 Jan T. Kleyna  <https://orcid.org/0000-0002-4734-8878>
 Daniela Lazzaro  <https://orcid.org/0000-0002-4470-6043>
 Michael Mommert  <https://orcid.org/0000-0002-8132-778X>
 Richard J. Wainscoat  <https://orcid.org/0000-0002-1341-0952>

References

Appenzeller, I., Fricke, K., Fürtig, W., et al. 1998, *Msngr*, **94**, 1
 Bufanda, E., Meech, K. J., Kleyna, J. T., et al. 2023, *PSJ*, **4**, 2
 Carpino, M., Milani, A., & Chesley, S. R. 2003, *Icar*, **166**, 248
 Chambers, K. C., Magnier, E. A., Metcalfe, N., et al. 2016, arXiv:1612.05560
 Chesley, S. R., Farnocchia, D., Pravec, P., & Vokrouhlický, D. 2016, IAU Symp. 318, Asteroids: New Observations, New Models (Cambridge: Cambridge Univ. Press), 250
 Chesley, S. R., & Yeomans, D. K. 2005, IAU Coll. 197, Dynamics of Populations of Planetary Systems (Cambridge: Cambridge Univ. Press), 289

Christensen, E. J., Carson Fuls, D., Gibbs, A., et al. 2016, AAS/DPS Meeting, **48**, 405.01
 Clark, B. E., Ockert-Bell, M. E., Cloutis, E. A., et al. 2009, *Icar*, **202**, 119
 Crovisier, J., Biver, N., Bockelee-Morvan, D., et al. 1995, *Icar*, **115**, 213
 Del Vigna, A., Faggioli, L., Milani, A., et al. 2018, *A&A*, **617**, A61
 Desch, S. J., & Jackson, A. P. 2021, *JGRE*, **126**, e06807
 Duncan, M., Levison, H., & Dones, L. 2004, Comets II, ed. M. C. Festou, H. U. Keller, & H. A. Weaver (Tucson, AZ: Univ. Arizona Press), 193
 Ettl, S., Farnocchia, D., Chamberlin, A. B., & Chesley, S. R. 2020, *Icar*, **339**, 113596
 Farnocchia, D. 2021, Small-Body Perturber Files SB441-N16 and SB441-N343, Tech. Rep. IOM 392R-21-005, Jet Propulsion Laboratory
 Farnocchia, D., Chesley, S. R., Chodas, P. W., et al. 2013, *Icar*, **224**, 192
 Farnocchia, D., Chesley, S. R., Chodas, P. W., et al. 2014a, *ApJ*, **790**, 114
 Farnocchia, D., Chesley, S. R., Milani, A., Gronchi, G. F., & Chodas, P. W. 2015, Asteroids IV, ed. P. Michel, F. E. DeMeo, & W. F. Bottke (Tucson, AZ: Univ. Arizona Press), 815
 Farnocchia, D., Chesley, S. R., Takahashi, Y., et al. 2021, *Icar*, **369**, 114594
 Farnocchia, D., Chesley, S. R., Tholen, D. J., & Micheli, M. 2014b, *CeMDA*, **119**, 301
 Farnocchia, D., Tholen, D. J., Micheli, M., et al. 2017, AAS/DPS Meeting, **49**, 100.09
 Fedorets, G., Micheli, M., Jedicke, R., et al. 2020, *AJ*, **160**, 277
 Feng, F., & Jones, H. R. A. 2018, *ApJL*, **852**, L27
 Fink, U. 2009, *Icar*, **201**, 311
 Gaia Collaboration, Prusti, T., de Bruijne, J. H. J., et al. 2016, *A&A*, **595**, A1
 Gaia Collaboration, Brown, A. G. A., Vallenari, A., et al. 2018, *A&A*, **616**, A1
 Gehrels, T., & Taylor, R. C. 1977, *AJ*, **82**, 229
 Granvik, M., Morbidelli, A., Jedicke, R., et al. 2018, *Icar*, **312**, 181
 Greenberg, A. H., Margot, J.-L., Verma, A. K., Taylor, P. A., & Hodge, S. E. 2020, *AJ*, **159**, 92
 Gunnarsson, M., Bockelee-Morvan, D., Biver, N., Crovisier, J., & Rickman, H. 2008, *A&A*, **484**, 537
 Hainaut, O. R., Micheli, M., Cano, J. L., et al. 2021, *A&A*, **653**, A124
 Hsieh, H. H., Novaković, B., Walsh, K. J., & Schörghofer, N. 2020, *AJ*, **159**, 179
 Ieva, S., Dotto, E., Mazzotta Epifani, E., et al. 2020, *A&A*, **644**, A23
 Jackson, A. P., & Desch, S. J. 2021, *JGRE*, **1**, e2020JE006706
 Jedicke, R., Granvik, M., Micheli, M., et al. 2015, Asteroids IV, ed. P. Michel, F. E. DeMeo, & W. F. Bottke (Tucson, AZ: Univ. Arizona Press), 795
 Jewitt, D., & Seligman, D. Z. 2022, arXiv:2209.08182
 Jordí, C., Gebran, M., Carrasco, J. M., et al. 2010, *A&A*, **523**, A48
 Królikowska, M. 2004, *A&A*, **427**, 1117
 Lagerkvist, C. I., & Lagerros, J. S. V. 1997, *AN*, **318**, 391
 Marschall, R., Markkanen, J., Gerig, S.-B., et al. 2020, *F&P*, **8**, 227
 Marsden, B. G., Sekanina, Z., & Yeomans, D. K. 1973, *AJ*, **78**, 211
 McMillan, R. S., Larsen, J. A., Bressi, T. H., et al. 2016, IAU Symp. 318, Asteroids: New Observations, New Models (Cambridge: Cambridge Univ. Press), 317
 Meech, K. J., & Belton, M. J. S. 1990, *AJ*, **100**, 1323
 Meech, K. J., Buie, M. W., Samarasinha, N. H., Mueller, B. E. A., & Belton, M. J. S. 1997, *AJ*, **113**, 844
 Meech, K. J., Fernández, Y., & Pittichová, J. 2001, AAS/DPS Meeting, **33**, 20.06
 Meech, K. J., & Jewitt, D. C. 1987, *A&A*, **187**, 585
 Meech, K. J., & Svoren, J. 2004, Comets II, ed. M. C. Festou, H. U. Keller, & H. A. Weaver (Tucson, AZ: Univ. Arizona Press), 317
 Meech, K. J., Schambeau, C. A., Sorli, K., et al. 2017, *AJ*, **153**, 206
 Micheli, M., Tholen, D. J., & Elliott, G. T. 2012, *NewA*, **17**, 446
 Micheli, M., Tholen, D. J., & Elliott, G. T. 2013, *Icar*, **226**, 251
 Micheli, M., Tholen, D. J., & Elliott, G. T. 2014, *ApJL*, **788**, L1
 Micheli, M., Farnocchia, D., Meech, K. J., et al. 2018, *Natur*, **559**, 223
 Mommert, M., Farnocchia, D., Hora, J. L., et al. 2014b, *ApJL*, **789**, L22
 Mommert, M., Hora, J. L., Farnocchia, D., et al. 2014a, *ApJ*, **786**, 148
 Ostro, S. J., Hudson, R. S., Benner, L. A. M., et al. 2002, Asteroids III, ed. W. F. Bottke, Jr. (Tucson, AZ: Univ. Arizona Press), 151
 Paganini, L., Mamma, M. J., Boehnhardt, H., et al. 2013, *ApJ*, **766**, 100
 Park, R. S., Folkner, W. M., Williams, J. G., & Boggs, D. H. 2021, *AJ*, **161**, 105
 Pravdo, S. H., Rabinowitz, D. L., Helin, E. F., et al. 1999, *AJ*, **117**, 1616
 Rafikov, R. R. 2018, *ApJL*, **867**, L17
 Reach, W. T., Kelley, M. S., & Vaubaillon, J. 2013, *Icar*, **226**, 777
 Seidelmann, P. K. 1977, *CeMec*, **16**, 165

- Seligman, D., & Laughlin, G. 2020, *ApJL*, **896**, L8
- Seligman, D. Z., Levine, W. G., Cabot, S. H. C., Laughlin, G., & Meech, K. 2021, *ApJ*, **920**, 28
- Senay, M. C., & Jewitt, D. 1994, *Natur*, **371**, 229
- Slemp, L. A., Meech, K. J., Bufanda, E., et al. 2022, *PSJ*, **3**, 34
- Snodgrass, C., Agarwal, J., Combi, M., et al. 2017, *A&ARv*, **25**, 5
- Spohn, T., Knollenberg, J., Ball, A. J., et al. 2015, *Sci.*, **349**, 2.464
- Taylor, A. G., Seligman, D. Z., MacAyeal, D. R., Hainaut, O. R., & Meech, K. J. 2022, arXiv:2209.15074
- Toliou, A., Granvik, M., & Tsirovoulis, G. 2021, *MNRAS*, **506**, 3301
- Trilling, D. E., Mommert, M., Hora, J. L., et al. 2018, *AJ*, **156**, 261
- Vereš, P., Farnocchia, D., Chesley, S. R., & Chamberlin, A. B. 2017, *Icar*, **296**, 139
- Vereš, P., Jedicke, R., Denneau, L., et al. 2012, *PASP*, **124**, 1197
- Vokrouhlický, D., Bottke, W. F., Chesley, S. R., Scheeres, D. J., & Statler, T. S. 2015, Asteroids IV, ed. P. Michel, F. E. DeMeo, & W. F. Bottke (Tucson, AZ: Univ. Arizona Press), 509
- Vokrouhlický, D., & Milani, A. 2000, *A&A*, **362**, 746
- Wainscoat, R., Chambers, K., Lilly, E., et al. 2016, IAU Symp. 318, Asteroids: New Observations, New Models (Cambridge: Cambridge Univ. Press), 293
- Wainscoat, R., Weryk, R., Ramanjooloo, Y., et al. 2020, AAS/DPS Meeting, **52**, 107.03
- Wierzbos, K., & Womack, M. 2020, *AJ*, **159**, 136
- Ye, J.-h., Zhao, H.-b., & Li, B. 2016, *ChA&A*, **40**, 54
- Yeomans, D. K., & Chodas, P. W. 1989, *AJ*, **98**, 1083
- Yeomans, D. K., Chodas, P. W., Sitarski, G., Szutowicz, S., & Królikowska, M. 2004, Comets II, ed. M. C. Festou, H. U. Keller, & H. A. Weaver (Tucson, AZ: Univ. Arizona Press), 137